



## COMPUTER MODELING OF PARTICLE PUSHING AND CLUSTERING DURING MATRIX CRYSTALLIZATION

R. K. SHELTON and D. C. DUNAND

Department of Materials Science and Engineering, Massachusetts Institute of Technology, Cambridge, MA 02139, U.S.A.

(Received 20 December 1995)

**Abstract**—Two-dimensional cellular automaton computer simulations were carried out to model the geometric interaction between mobile, equiaxed particles and growing matrix grains, thus simulating crystallization (respectively, recrystallization, phase transformation or solidification) of a matrix material containing a mobile second phase (e.g. solid particles, liquid droplets or gas bubbles). The model allows the study of particle pushing by growing grains, which leads to particle accumulation and clustering at grain boundaries and triple points, and concomitant particle depletion within grains. Parameters explored are particle area fraction, particle settling speed, particle cluster mobility and grain nucleation rate under continuous nucleation conditions. These parameters are found to strongly affect the particle spatial distribution and clustering during and after crystallization. Conversely, the particles have no measurable effect on the grain shape or size. Finally, site-saturated nucleation at the boundaries of the simulation field is investigated, simulating e.g. solidification from crucible walls or recrystallization from sample edges. Pronounced clustering of particles takes place at grain boundaries and is further accentuated by particle settling. Copyright © 1996 Acta Metallurgica Inc.

### 1. INTRODUCTION

Nucleation, growth and impingement of spherical grains describe a variety of transformation phenomena in materials science, e.g. crystallization, recrystallization, eutectic solidification and some allotropic phase transformations. Analytical solutions by Johnson and Mehl [1], Avrami [2, 3] and Kolmogorov [4] (JMAK) describe the volume fraction of crystallized grains as a function of time. However, these types of closed-form solutions are available only for simple cases such as continuous nucleation, site-saturated nucleation and continuously varying nucleation rates [5], and they do not describe the resulting grain geometry and topology. Computer simulations have been used by many researchers to explore more complex conditions (e.g. time-dependent nucleation or growth rates, localized heterogeneous nucleation, complex spatial boundary conditions for castings) as well as grain geometry and topology (e.g. grain size average and distribution, grain aspect ratio, grain boundary length and triple point geometry). They have been applied to twinning [6], allotropic phase transformations [7], crystallization or recrystallization [8–21] and solidification [22–35].

For many two-phase materials (e.g. precipitation- or dispersion-strengthened alloys and metal-, ceramic- or polymer-matrix composites), crystallization or recrystallization of the matrix occurs in the presence of a second phase which is inert (i.e. insoluble and neither growing nor crystallizing). In

the simplest case where the second phase is immobile, the kinetics of recrystallization or crystallization of the matrix can be strongly affected by the second phase through heterogeneous nucleation of matrix grains and through blocking of the motion of grain boundaries (Zener pinning and/or geometric impingement) [18]. Computer simulations have been used by many investigators [36–41] to examine the effects of a uniform dispersion of small equiaxed particles on grain nucleation and grain boundary pinning during recrystallization. Other investigators [5, 42–45] also simulated the recrystallization of a metal containing spatially nonuniformly distributed particles (e.g. stringers in rolled metals). Finally, computer models have been used to study the impingement effect between growing grains and continuous fibers [46–48], discontinuous fibers [49, 50] or equiaxed particles [49–51].

A more complex situation arises if inert particles are mobile and can be pushed by the pressure exerted by a moving grain boundary. While, to the best of our knowledge, this case has not been studied by computer simulation, many experimental observations of particle pushing by growing grains have been made. In what follows, we give a few examples of particle pushing classified by matrix transformation and particle state. For a matrix undergoing a solid–solid transformation (e.g. allotropic transformation, recrystallization or crystallization from the amorphous state), particle pushing by moving grain boundaries has been reported for solid particles [52–55], liquid droplets [53] and gas bubbles [56];

diffusional creep of metals containing fine precipitates can also lead to solid particle pushing by moving grain boundaries [57, 58]. For a matrix undergoing a liquid–solid transformation (i.e. solidification), pushing of solid particles by grains has been observed for metals, water and organic liquids, as reviewed in [59–61]. Pushing of liquid droplets by grains is also possible during solidification of systems containing immiscible liquids with different melting points [59, 60]. Finally, gas bubbles can be pushed by grains (e.g. solidification of water with air bubbles or solidification of semi-killed steel containing CO bubbles [62]). When homogeneously distributed particles are pushed during recrystallization or solidification, grain boundaries are enriched with particles and grain interiors are depleted. The resulting inhomogeneous microstructure is usually undesirable: for solidified metal matrix composites for instance, particle-rich regions are embrittled, while particle-poor regions are weakened.

In the present article, we use cellular automata simulations to examine particle pushing by growing grains nucleated under homogenous, continuous conditions or heterogenous, site-saturated conditions. We investigate the effect of grain nucleation rate, particle area fraction, particle settling rate and particle mobility upon the particle distribution and the composite final microstructure.

## 2. COMPUTATIONAL PROCEDURES

We use a two-dimensional cellular automaton approach to simulate recrystallization, introduced by Hesselbarth and Göbel [15] for single-phase materials and extended by Pezzee and Dunand [49] for two-phase materials (i.e. a matrix containing immobile, inert particles or fibers). Two- and three-dimensional cellular automata have also been used for solidification simulation without particles by Brown and coworkers for dendritic growth [25–27] and by Zhu and Smith [28, 29] and Rappaz and coworkers [30–35] for equiaxed and dendritic growth. For brevity, we will use in the following the general term “crystallization” to cover the particular cases of crystallization, recrystallization, solidification and transformation.

Our cellular automaton consists of a two-dimensional field of 65,536 ( $256^2$ ) square cells oriented along orthogonal axes with periodic boundary conditions. Each cell, which can represent either the matrix or a second-phase particle, is updated at discrete time-steps according to local, deterministic topological rules. Matrix cells, which can have two possible states (crystallized or uncrystallized), are subjected during each time-step to two sequential events: growth and nucleation.

In the nucleation event, nuclei consisting of a single crystallized cell are distributed randomly on the field (but with no pair of nuclei as nearest neighbor), according to two possible regimes. In the first regime,

corresponding to homogenous nucleation without particle-stimulated nucleation, nuclei are distributed at each time-step over the whole field at a constant area fraction. The total number of new nuclei added to the field thus decreases with increasing time-steps as the crystallized area fraction (which is unavailable for nuclei) increases. The other nucleation regime investigated is local site saturation, where all nuclei are distributed in the first time-step within a single-cell-wide strip at the four borders of the field. This regime simulates heterogeneous solidification from the walls of a casting.

In the growth event, each crystallized matrix cell remains unchanged, while those uncrystallized matrix cells with at least one of their nearest neighbors belonging to a grain become part of that grain. If an uncrystallized cell has crystallized neighbors from different grains, it becomes part of any of the competing grains with the same probability. As described in more detail in [15, 49], an alternating neighborhood of six cells is chosen for the growth event, resulting before impingement in equiaxed, octagonal grain shape. This shape approximates the circular (respectively, spherical) shape observed during crystallization, recrystallization and eutectic solidification of isotropic materials; however, more complex rules must be defined for dendritic solidification, as shown in e.g. [25, 33].

Particle cells, which have a single state, are assigned randomly on the whole field at time  $t = 0$ . A particle does not move if it is not in contact with a matrix grain, i.e. if none of its eight nearest neighboring cells belongs to a grain. However, if a particle cell (say cell A) has at least one neighbor as a crystallized grain cell, it is moved to a neighboring uncrystallized matrix cell (say cell B) by assigning to cell A the uncrystallized matrix status and to cell B the particle cell status. If more than one uncrystallized neighbor cell exist, the particle cell moves randomly to any of the available uncrystallized cells. However, to prevent the particle (now in cell B) from moving back to the position (cell A) it left in the previous time-step (which can lead to early engulfing of the particle by the grain), the uncrystallized neighbor cell which has the most crystallized neighbors (in most cases cell A) is not considered as a new site for the particle, unless it is the only possibility. If all the neighboring cells are crystallized or occupied with other particles, the particle is considered engulfed by the grain and/or immobilized by neighboring particles.

As particles accumulate at a moving grain boundary, they contact and form clusters, defined as an aggregate of at least two particles. We consider two extreme cases: zero mobility of clusters and infinite mobility of clusters. In the former case, as soon as two particles contact, the resulting cluster becomes immobile and is engulfed by the advancing grain. This scenario corresponds to the case of crystallization with particle coalescence (e.g. for

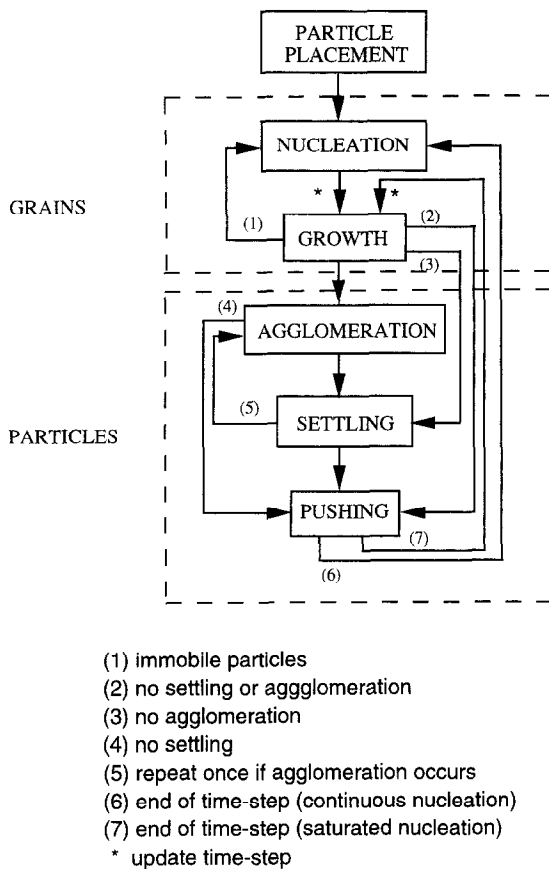


Fig. 1. Program flowchart with various substeps, each of which is applied to the whole field.

droplets and bubbles): since the particle mobility is inversely proportional to the third or fourth power of the particle radius [55], coalescence strongly reduces the aggregate mobility. In the second case, particle clusters are assumed fully mobile (e.g. for solid particles which do not merge upon contact during matrix crystallization [52–55] or solidification [59–61]). For a given time-step, the particle pushing procedure is repeated until all particles in the cluster have had the opportunity to move once (and only once).

Finally, settling or floating of particles can occur during solidification when particles experience a buoyancy force significantly larger than the viscous drag force, as often observed during gravity or centrifugal casting of liquid metals containing ceramic particles or gas bubbles [59–63]. In the present simulation another substep is added to

simulate the effect of settling: each particle moves randomly to any of the three neighboring cells directly below its position, unless they are occupied by a grain or another particle.

Figure 1 shows a flowchart of a complete time-step consisting of the substeps described above, each of which is applied to the whole field before the next substep is considered. As indicated by arrows, some or all substeps related to the particles (i.e. pushing, clustering and settling) can be bypassed. After each time-step, the area fraction of crystallized matrix  $x$  is computed as the ratio of crystallized matrix area to total matrix area. Furthermore, for each particle the dimensionless distance to the nearest particle  $z$  normalized by the particle length is determined. At the end of the simulation, the grain size  $A$  (measured in number of cells) and the grain aspect ratio  $R$ , defined as the ratio (larger than 1) of the projections of the grain along the two orthogonal axes determined by the cell shape, are calculated for each grain. All grain statistical results were determined from at least two simulations carried out with the same parameters, but different spatial distributions of particles and nuclei.

Various parameters related to grains and particles were investigated: grain nucleation regime (homogenous or site-saturated), grain nucleation rate  $N$ , particle area fraction  $f$ , particle cluster mobility  $m$  ( $m = 1$  corresponds to full aggregate mobility,  $m = 0$  to zero mobility) and particle settling ratio  $s$ . The latter parameter is defined as the number of times the settling substep (Fig. 1) is repeated within a single time-step, i.e. the ratio of particle settling rate to grain growth rate. Each parameter was individually varied while keeping the remaining constant at the baseline values given in Table 1.

### 3. RESULTS

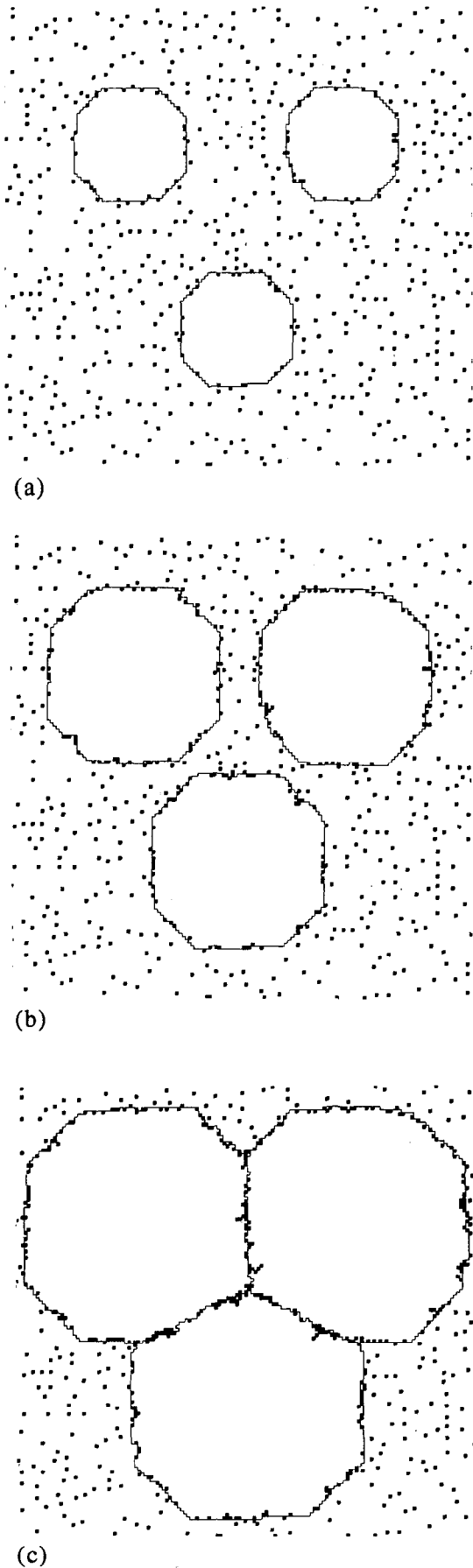
Figures 2(a)–(c) illustrate the growth and impingement of three isolated grains nucleated simultaneously in a matrix containing nonsettling, nonagglomerating particles with area fraction  $f = 0.0625$ . The particles are represented by filled cells and the grain borders are shown as lines. In the following, we use the term “border” for the interface between a grain and the uncrystallized matrix and the term “boundary” for the interface between two crystallized grains. In the early stage of growth [Fig. 2(a)] individual particles are pushed by the grain borders. Just before grain impingement [Fig. 2(b)] particles have accumulated at the borders and form

Table 1. Grain and particle parameters investigated under conditions of continuous nucleation (baseline values are in bold characters)

Grain nucleation rate $N^a$	$2 \times 10^{-4}$	<b><math>4 \times 10^{-4}</math></b>	$1.6 \times 10^{-3}$	$6.4 \times 10^{-3}$
Particle area fraction $f^b$	0	0.015625	0.03125	<b>0.0625</b>
Particle cluster mobility $m^b$	0	<b>1</b>		
Particle settling ratio $s^b$	<b>0</b>	1	3	5

<sup>a</sup>Nuclei per unit area and time.

<sup>b</sup>Dimensionless parameter.



individual clusters. At the end of grain impingement [Fig. 2(c)], all particles originally within the triangle formed by the three grain nuclei have been trapped at the newly formed grain boundaries.

In Fig. 3 the cellular field is shown for continuous nucleation conditions with the baseline conditions ( $N_0 = 4 \times 10^{-4}$  nuclei per unit area and time,  $f = 0.0625$ ,  $m = 1$ ,  $s = 0$ ) at two different stages of crystallization. When about half the field is crystallized [Fig. 3(a)], most grain borders have collected significant quantities of particles. However, grain boundaries created at an early stage by the impingement of two grains nucleated close to each other are relatively free of particles. The fully crystallized structure [Fig. 3(b)] exhibits a highly inhomogeneous particle distribution: most particles are agglomerated in clusters and large particle concentrations exist at grain triple points. However, as shown in Figs 4(a) and (b), an increased nucleation rate ( $N = 16 N_0$ ) leads to a more homogeneous distribution of particles, as expected from the increased total grain boundary length.

Figure 5 shows the average particle nearest neighbor distance  $z_{av}$  (normalized by the initial value  $z_{av,0}$ ) as a function of time for the three particle area fractions explored. The clustering of particles leads to a decreasing value of  $z_{av}$  with time and the effect is stronger the higher the particle content. In Fig. 6 the distribution of particle nearest-neighbor distance  $z$  is given for three different times. As crystallization progresses, the distribution first broadens, because some of the particles are pushed, and then narrows, because most particles are in clusters. The average value  $z_{av}$  steadily decreases, as indicated on the top of Fig. 6 and as also plotted in Fig. 5.

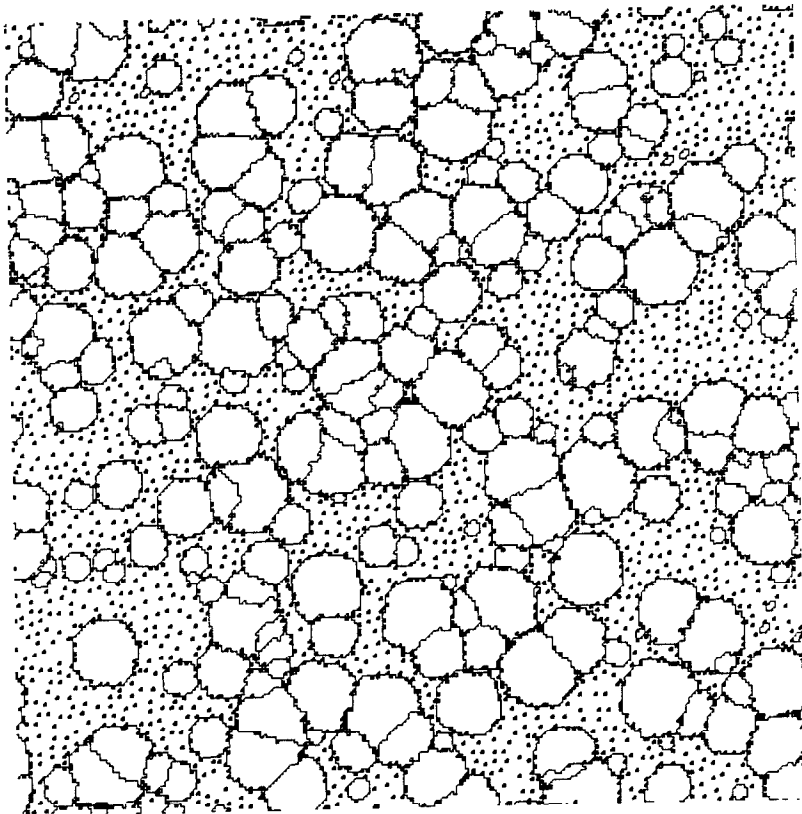
As shown in Fig. 7, the area fraction of crystallized grains  $x$  is found to vary with time  $t$  according to the classical JMAK equation:

$$x = 1 - \exp(-kt^n), \quad (1)$$

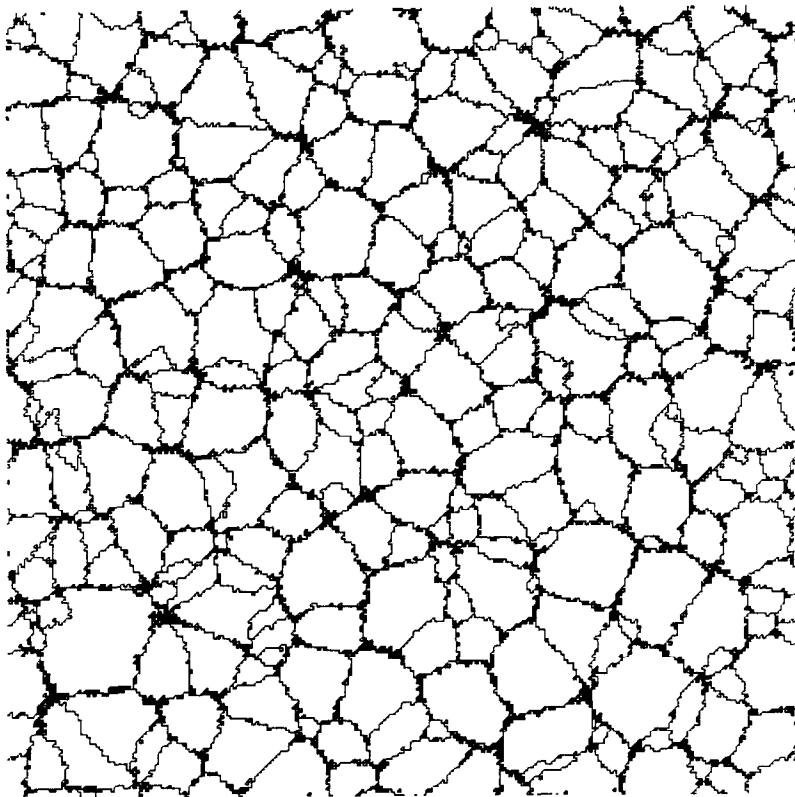
where  $n$  is the Avrami exponent and  $k$  is a constant containing the nucleation rate  $N$  and the growth rate  $G$ . For all particle and grain parameters explored (Table 1), the simulations give an Avrami exponent  $n = 3.0$  within the interval  $0 < x < 0.98$ , as analytically predicted by the JMAK theory for two-dimensional grain growth under continuous nucleation conditions. We note that time, expressed in units of time-steps, can also be considered as a dimensionless parameter: a time-step is the unit time for which a grain radius grows by a unit length.

Grain size average and distribution as well as grain aspect ratio average and distribution are insensitive to the particle area fraction. The average grain size is  $\bar{A} = 212 \pm 2$  cells, in agreement with values reported

Fig. 2. Growth of three isolated grains in the presence of mobile particles ( $f = 0.0625$ ,  $m = 1$ ,  $s = 0$ ): (a) after 18 time-steps, (b) after 28 time-steps and (c) after 38 time-steps.

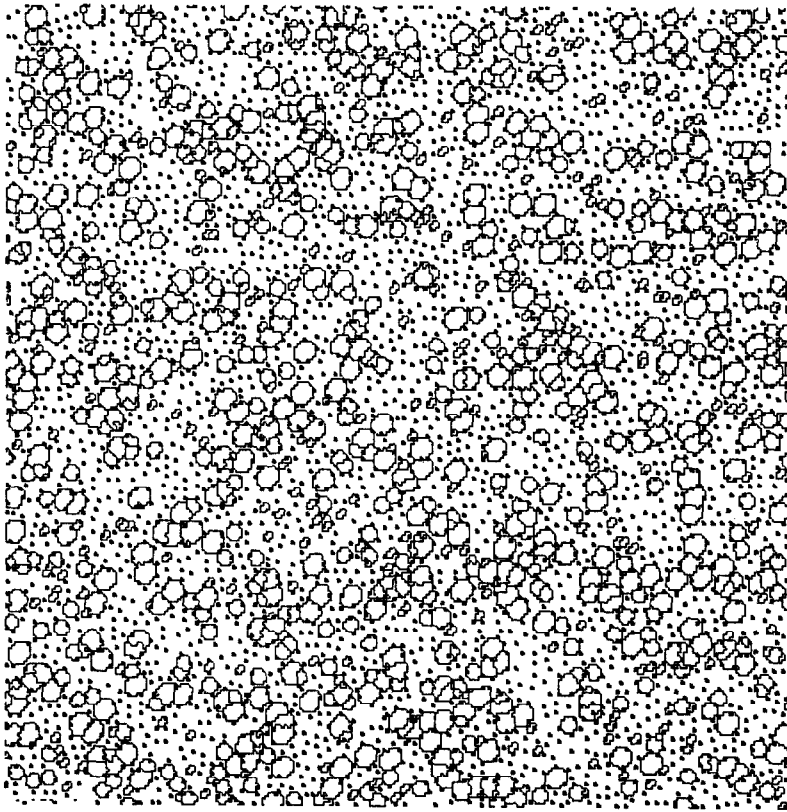


(a)

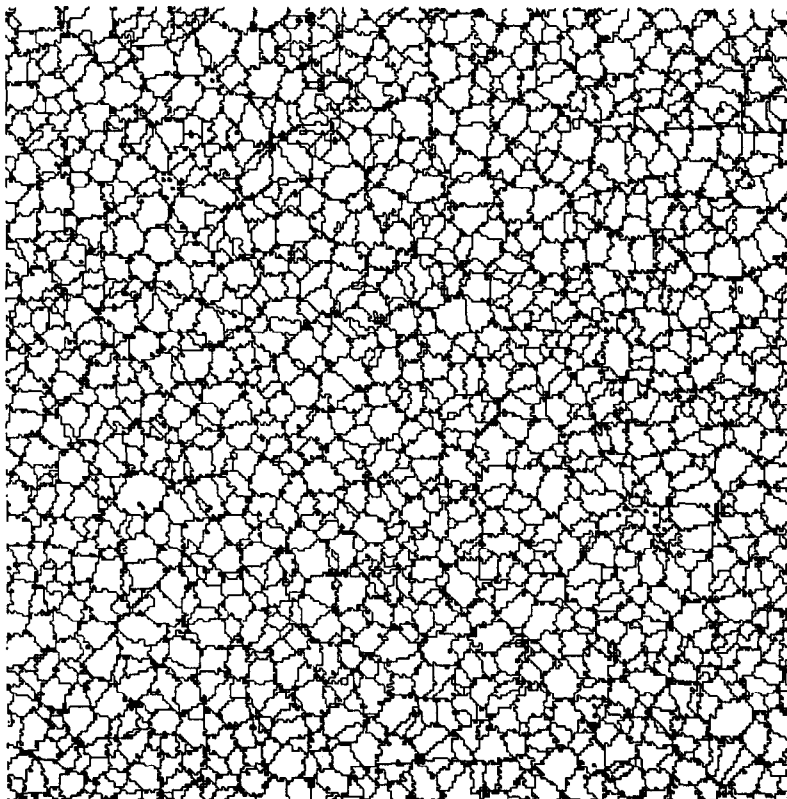


(b)

Fig. 3. Field containing mobile particles for baseline parameters ( $N = N_0 = 4 \times 10^{-4}$  nuclei per unit area and time,  $f = 0.0625$ ,  $m = 1$ ,  $s = 0$ ): (a) after 13 time-steps and (b) after 24 time-steps.



(a)



(b)

Fig. 4. Field containing mobile particles ( $N = 16 N_0$ ,  $f = 0.0625$ ,  $m = 1$ ,  $s = 0$ ): (a) after 3 time-steps and (b) after 8 time-steps.

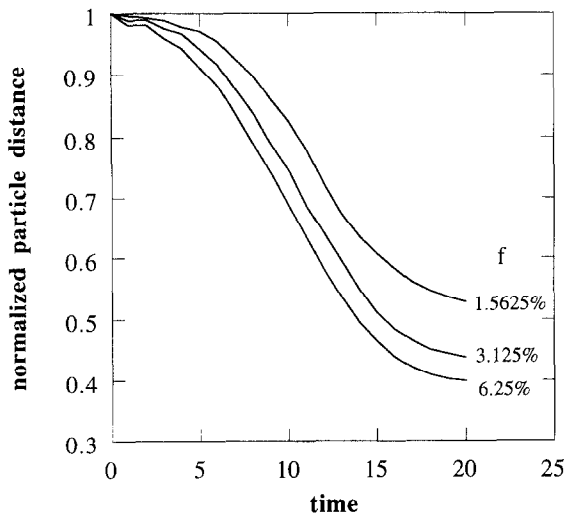


Fig. 5. Time dependence of the average interparticle distance  $z_{av}$  (normalized by  $z_{av,0}$ , the value at  $t = 0$ ) for different particle area fractions  $f$  ( $N = N_0$ ,  $m = 1$ ,  $s = 0$ ).

earlier [49] for immobile particles and close to the theoretical values given by Gilbert [64] for a matrix crystallizing in the absence of particles:

$$\bar{A} = 1.1371 (G/N)^{2/3}, \quad (2)$$

which predicts  $\bar{A} = 217$  cells for values of  $G = 1.055$  cell per unit time and  $N = 4 \times 10^{-4}$  nuclei per unit area and time. The former parameter was found experimentally by plotting the area of a single octagonal grain as a function of time and determining the growth rate of a circular grain of the same area ( $G = 1$  cell per unit time would be expected for circular grains).

Figure 8 corresponds to the case where particles are settling at a rate five times higher than the grain

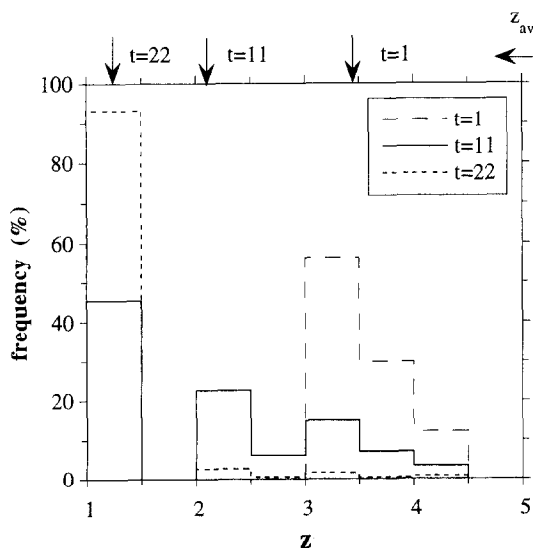


Fig. 6. Distribution of interparticle distance  $z$  (normalized by particle size) as a function of time for baseline parameters ( $N = N_0$ ,  $f = 0.0625$ ,  $m = 1$ ,  $s = 0$ ). The respective average values  $z_{av}$  are indicated with arrows.

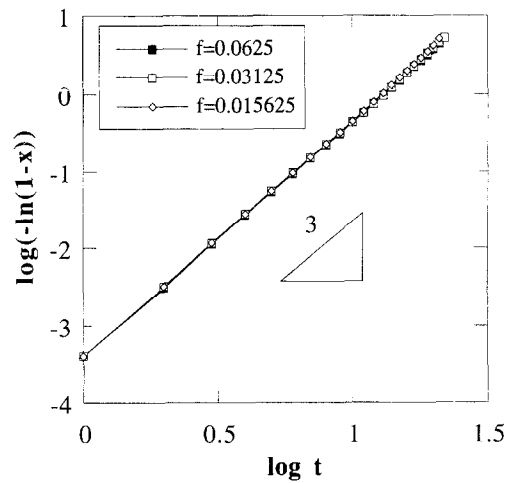


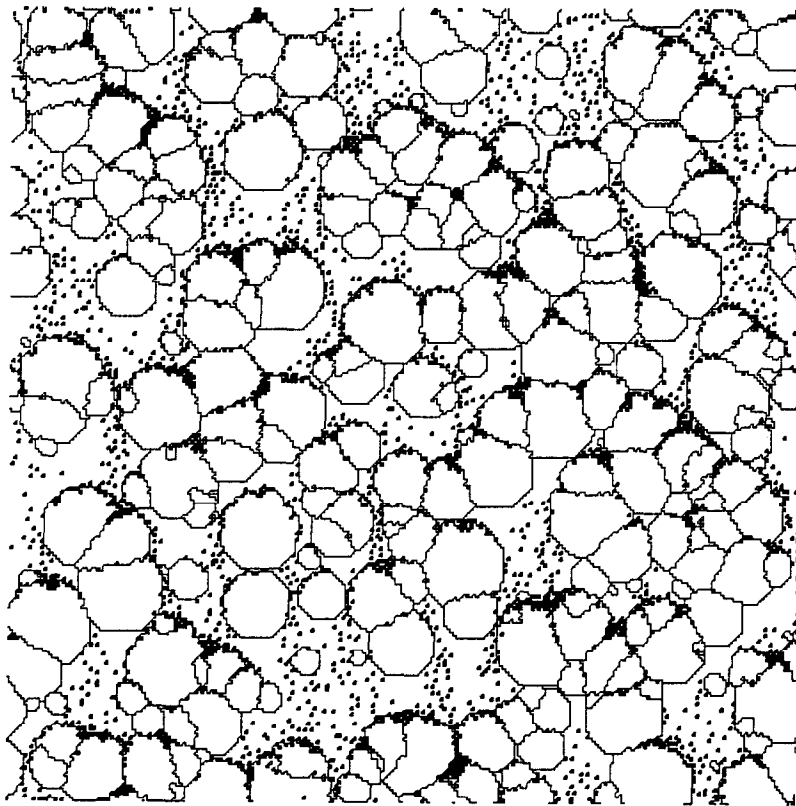
Fig. 7. JMAK plots of the matrix fraction crystallized  $x$  as a function of time  $t$  for different particle area fractions  $f$  ( $N = N_0$ ,  $m = 1$ ,  $s = 0$ ).

growth rate ( $s = 5$ ) with the other parameters at baseline value. With about half of the structure crystallized [Fig. 8(a)], particles have settled on the grain borders moving in the direction opposite to the settling direction, while borders moving in the same direction are devoid of particles. As a result, the final microstructure [Fig. 8(b)] exhibits pronounced agglomeration of particles. Figure 9 shows the effect of different settling ratios  $s$  on the time dependence of the average particle nearest neighbor distance  $z_{av}$ . Also shown in this figure is the case where particles settle in the absence of any grains pushing them ( $s = 1$ ,  $N = 0$ ).

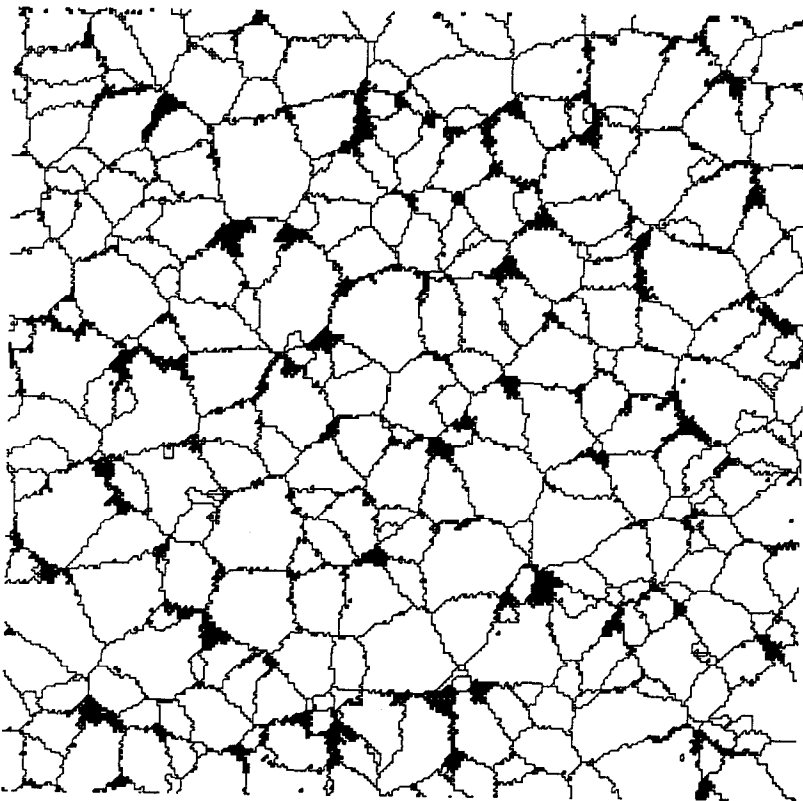
Figures 10(a) and (b) show the microstructure resulting from zero particle cluster mobility ( $m = 0$ ): clusters form early and are engulfed within the growing grains [Fig. 10(a)], resulting in a final structure showing a rather homogenous distribution of particle clusters [Fig. 10(b)]. The time dependence of  $z_{av}$  is not reported, because it is not significantly different from that of full cluster mobility ( $m = 1$ , Fig. 5).

For the standard particle area fraction  $f = 0.0625$ , no change in grain area average or distribution is found upon settling ( $s = 1, 3, 5$ ) or upon cluster immobility ( $m = 0$ ). For all cases investigated, the average grain aspect ratio is near unity, as expected for equiaxed grains growing within a field of equiaxed particles [49] and the distribution of grain aspect ratios is independent of the simulation parameters.

To simulate solidification from die walls, site-saturated nucleation at the edge of the square field was considered for a particle area fraction  $f = 0.03125$  with 150 grains nucleated during the first time-step only. As seen in Fig. 11 for the case of nonsettling particles ( $s = 0$ ), columnar growth of grains results from competition between grains nucleated simultaneously. Particles are initially pushed by each of the four fronts [Fig. 11(a)] and are



(a)



(b)

Fig. 8. Field containing mobile particles under rapid settling conditions ( $N = N_0$ ,  $f = 0.0625$ ,  $m = 1$ ,  $s = 5$ ): (a) after 13 time-steps and (b) after 22 time-steps. The settling direction is indicated with an arrow.

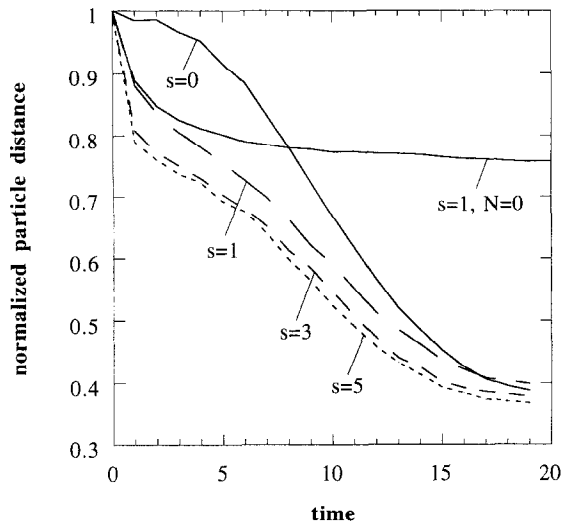


Fig. 9. Time dependence of the average interparticle distance  $z_{av}$  (normalized by  $z_{av,0}$ , the value at  $t=0$ ) for different particle settling rates  $s$  ( $N = N_0$ ,  $f = 0.0625$ ,  $m = 1$ ).

then trapped at grain boundaries [Fig. 11(b)]. The final microstructure exhibits a heavily clustered distribution of particles located mainly along the grain boundary diagonals formed upon the impingement of grains growing in different directions. When particles settle more rapidly than the growth of grains ( $s = 3$ ), particles accumulate mostly along the front moving in the direction opposite to the settling direction [Fig. 12(a)]. Pronounced accumulation results at the grain boundaries corresponding to this front [Fig. 12(b)], resulting in a microstructure exhibiting a few large clusters, while the rest of the field is virtually particle-free [Fig. 12(c)].

#### 4. DISCUSSION

While the qualitative agreement between the simulated microstructures presented above and experimental microstructures (e.g. [59, 65–67]) is encouraging, our simulations can provide only a rough model of real materials systems, because of the many simplifying assumptions listed below:

- octagonal grain shape of isolated grains: whereas this shape is close to the ideal circular shape expected from equiaxed growth, the octagonal grain shape in the present simulation reflects the orthogonal nature of the cellular grid and the simple growth rule used. Furthermore, while circular grains are observed in the two-dimensional crystallization of amorphous thin films [68], only eutectic alloys exhibit circular (respectively, spherical) grains upon solidification.
- constant and isotropic growth rate: this condition corresponds to isothermal growth and also assumes that the particles have no pinning effect on the grain boundaries and that growth is independent of direction.

- constant nucleation rate and random nucleation sites: in real systems, nucleation often occurs at heterogenous sites (previous grain boundaries for recrystallization, particles for recrystallization and solidification, container walls for solidification) and is therefore neither random nor constant.
- uniform particle size and shape: real systems typically display a continuous distribution of particle size and shape and therefore a distribution of particle mobility.
- limited number of grains: in a  $256^2$  array, a total of *ca* 300 grains are formed for the baseline nucleation rate, thus limiting the statistical accuracy of each simulation. We used periodic boundary conditions to mitigate that problem and established that repeatability was good by carrying multiple simulations under the same parametric conditions.

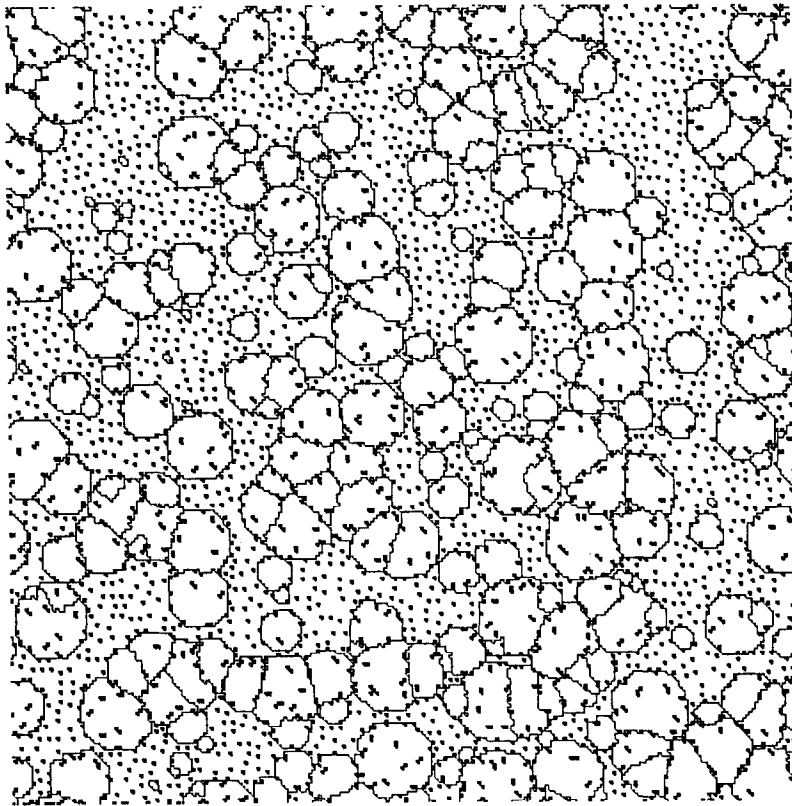
Finally, the two-dimensional simulations in the present paper are applicable only to cases where grain thickness is much smaller than grain diameters, e.g. for crystallization of thin films or slender bodies such as plates and shells. As discussed by Humphreys and Hatherly [18], extrapolation from two- to three-dimensional results may lead to erroneous conclusions.

Despite the above reservations, we believe that computer simulations of structural evolution, such as those presented above or published by the authors cited in the Introduction, are useful and relevant because they provide a qualitative and quantitative understanding of elementary mechanisms (e.g. particle pushing, settling and agglomeration) operative in a complex environment (e.g. impinging particles and impinging grains) and because they allow the investigation of each system parameter separately, a difficult task in real materials systems. As pointed out by Humphreys and Hatherly [18], “perhaps at this time, one of the most useful roles of computer simulations is to draw attention to areas where further theoretical and experimental work are needed”.

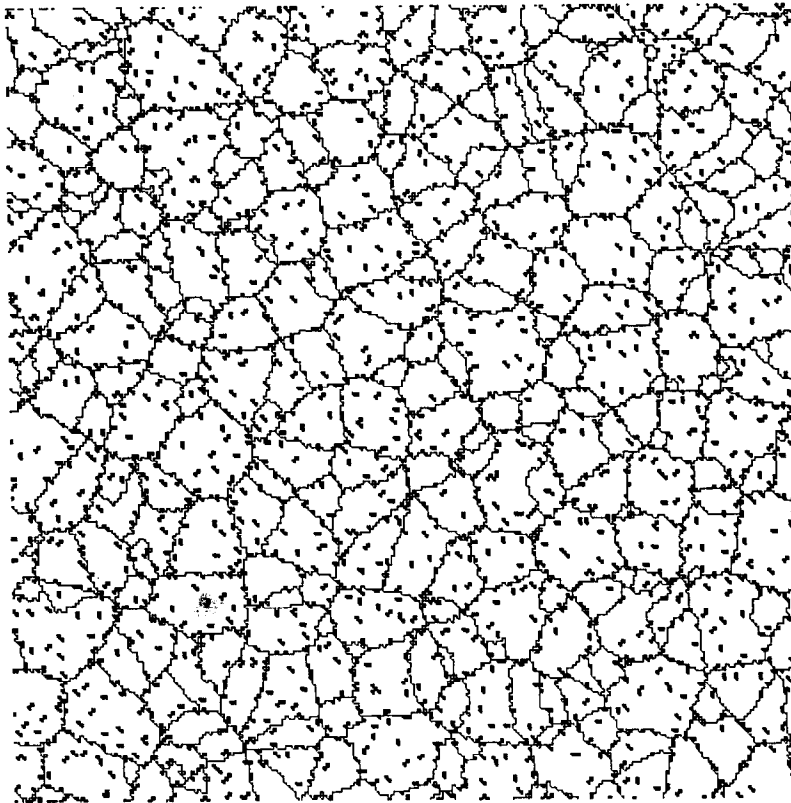
##### 4.1. Single grains

Figures 2(a)–(c) illustrate the mechanisms of particle pushing and clustering for the simplified case of three equidistant grains nucleated simultaneously. As reflected by the increasingly ragged morphology of the borders with increasing time, particles have a small but noticeable effect on the morphology of grain borders pushing them. This effect stems from the geometric impingement of the particle clusters, explored in detail in a previous publication [49] for immobile particles.

Figures 2(a)–(c) also show that, despite the initially random particle distribution, agglomeration of particles rapidly occurs at the grain borders. These clusters are originally only a single particle thick



(a)



(b)

Fig. 10. Field containing mobile particles with zero cluster mobility ( $N = N_0$ ,  $f = 0.0625$ ,  $m = 0$ ,  $s = 0$ )  
(a) after 13 time-steps and (b) after 22 time-steps.

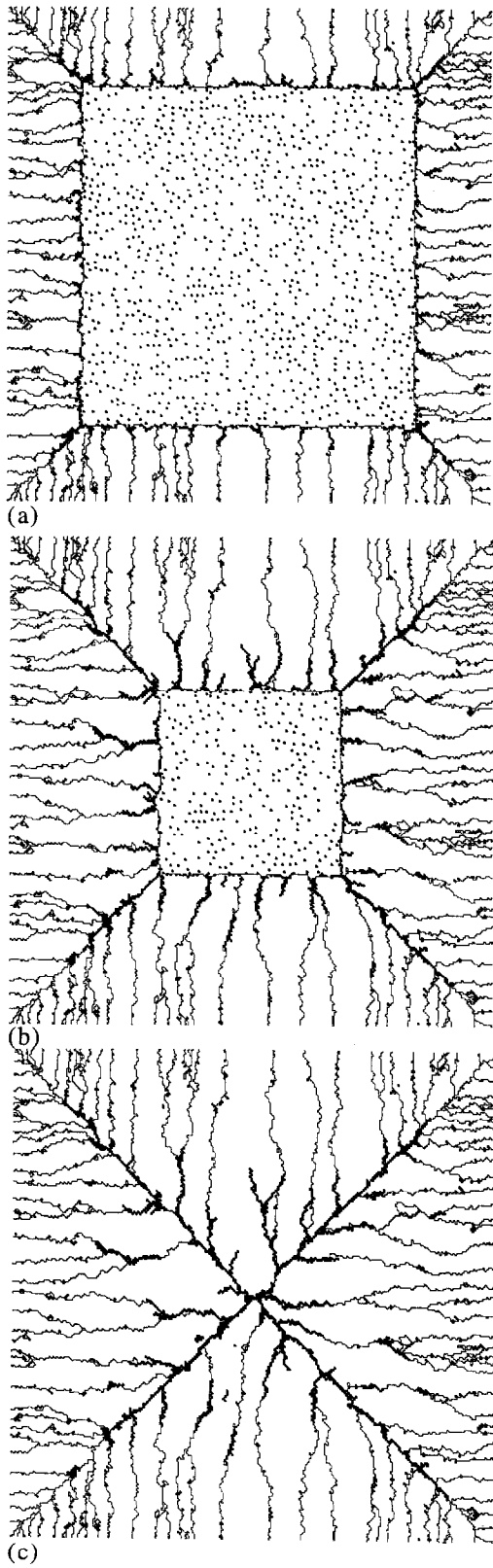


Fig. 11. Field containing mobile particles with 150 grains nucleated under site-saturated conditions at the field borders ( $f = 0.03125$ ,  $m = 1$ ,  $s = 0$ ): (a) after 40 time-steps, (b) after 80 time-steps and (c) after 128 time-steps.

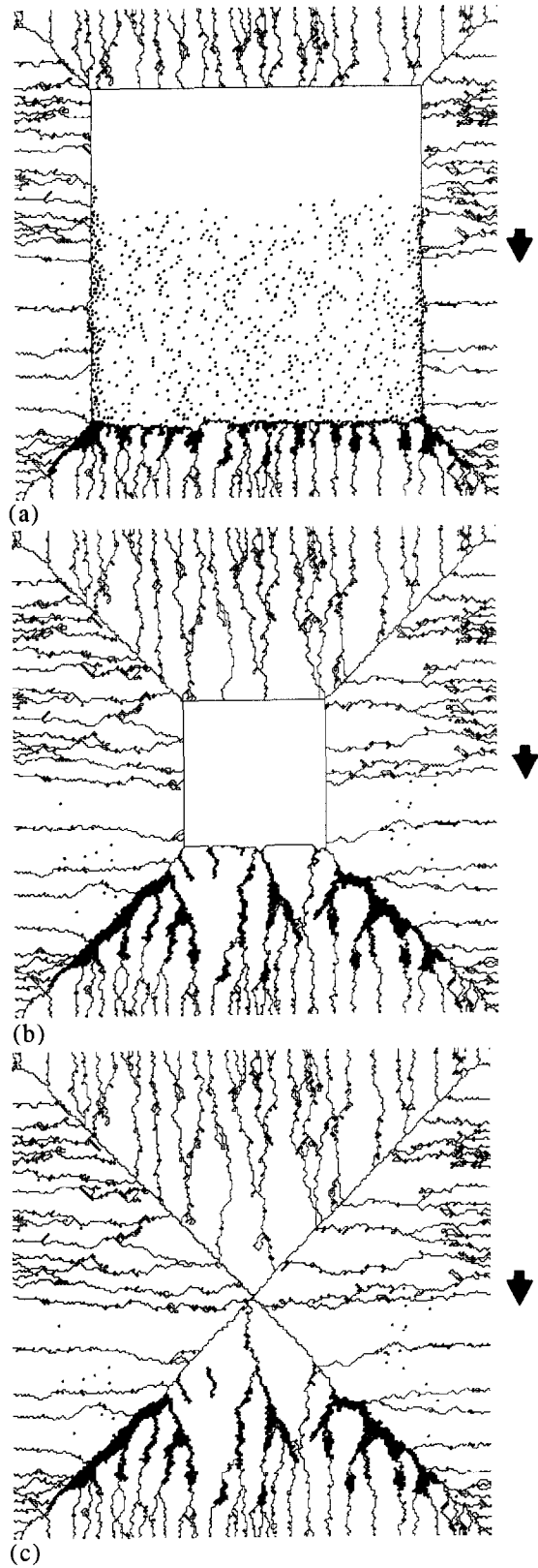


Fig. 12. Field containing mobile, settling particles with 150 grains nucleated under site-saturated conditions at the field borders ( $f = 0.03125$ ,  $m = 1$ ,  $s = 3$ ): (a) after 40 time-steps, (b) after 80 time-steps and (c) after 128 time-steps. The settling direction is indicated with an arrow.

[Fig. 2(a)], since motion of particles parallel to the border during pushing favors spreading of the cluster. However, as particle clusters grow, the rate of particle accumulation by each cluster increases with its projected area, while the rate of lateral spreading remains constant. Therefore, clusters thicken and become partially engulfed by the grain pushing them [Fig. 2(b)], but are still mobile since the computing algorithm (Fig. 1) repeats the pushing step until all particles in the clusters have had the opportunity to move once. In rare cases for large clusters impinging deeply into grains, engulfing of individual particles occurs [Fig. 8(b)].

Particles can be trapped at grain boundaries when two flat grain borders growing in opposite directions capture the respective particles as a result of a frontal collision (upper two grains in Fig. 2). However, in real systems, grain borders are rarely flat and the collision of two borders usually leads to a groove. Particles can be pushed without trapping by such grooves when borders move at a right angle to each other, as seen in Fig. 2(c); the groove eventually evolves into a flat front. As illustrated in Fig. 2(c), particles then collect at grain triple points, since it is the last place to crystallize.

#### 4.2. Continuous nucleation

**4.2.1. Effect of particle and grain density.** As shown in Fig. 2, particle clustering takes place in two successive stages: (i) particle collection by a grain border from a grain growing freely in the matrix and (ii) particle concentration at triple points by grooves resulting from the collision of two grains. If particles are trapped as soon as two borders collide to form a grain boundary or if the grain nucleation rate is high enough that full crystallization is reached shortly after significant grain impingement occurs (Fig. 4), stage (ii) is inactive and particles are randomly distributed on the grain boundaries. Assuming that all grains have the same area  $A$ , the average density of particles at grain boundaries  $\rho$  (expressed in particles per unit length) is:

$$\rho = \frac{2 \cdot f \cdot A}{a \cdot P}, \quad (3)$$

where  $f$  is the particle area fraction,  $a$  is the particle area and  $P$  is the grain perimeter, which can be expressed as:

$$P = k \cdot A^{1/2}, \quad (4)$$

where  $k$  is a geometric factor depending upon the shape of the grains. For squares,  $k = 4$ , and for hexagons,  $k = (8\sqrt{3})^{1/2} = 3.72$ . Introducing equation (3) into (4) gives:

$$\rho = \frac{2 \cdot f \cdot A^{1/2}}{a \cdot k}. \quad (5)$$

For  $\rho = 1$ , clustering is unavoidable since the totality of the boundaries length is covered by particles. To reduce clustering, the particle area fraction  $f$  can

be decreased or the particle area  $a$  or the grain nucleation rate  $N$  (which is inversely proportional to the grain area  $A$ ) increased.

With parameters corresponding to the standard conditions in Fig. 3 ( $k = 3.72$ ,  $f = 0.0625$ ,  $a = 1$  cell,  $A = \bar{A} = 212$  cells), equation (5) predicts  $\rho = 0.49$  cell<sup>-1/2</sup>, i.e. particles cover almost half the line length provided by the grain boundaries. While the grains exhibit a broad size distribution and the assumption  $A = \bar{A}$  is thus very approximate, this simple calculation shows that clustering is expected to be mild for all particle area fractions examined in the present simulations, if particles are trapped as soon as their respective grain borders collide with other grain borders. Figure 3(a) indeed shows that clusters at grain borders are small, typically two cells, for grains which have not yet impinged with other grains. For the parameters corresponding to Fig. 4 with high grain nucleation rate  $N = 16 N_0$  (values as above, except  $A = \bar{A} = 36 \pm 0.1$  cells); equation [5] predicts  $\rho = 0.20$  cell<sup>-1/2</sup>. Clustering in the final microstructure [Fig. 4(b)] is thus expected to be significantly reduced as compared to the standard conditions [Fig. 3(b)] with a higher particle grain boundary density  $\rho = 0.49$  cell<sup>-1/2</sup>.

In stage (ii), particles are pushed towards grain boundary nodes (triple or quadruple points) by grains which have impinged with each other, so that the corresponding grain boundaries are devoid of particles. Assuming a regular lattice of monosized grains with all particles at nodes, the density of particles at grain boundary nodes is:

$$\rho' = \frac{m}{M} \cdot \frac{f \cdot A}{a}, \quad (6)$$

where  $m$  is the number of grains meeting at a node and  $M$  is the number of sides of the grains. For square grains,  $m/M = 1$  and for hexagonal grains,  $m/M = 1/2$ . With  $m/M = 1/2$ ,  $f = 0.0625$  and  $\bar{A} = 212$  cells, equation (6) predicts  $\rho' = 6.6$ , i.e. about seven particles per triple points. Figure 3(b) indeed shows that virtually all grain boundary nodes exhibit large clusters, with particles spreading from the node along each grain boundary. As a result, grain boundaries are mostly devoid of particles near their middle points between two nodes. For the smallest particle area fraction ( $f = 0.015625$ ) or highest nucleation rate ( $N = 16 N_0$ ,  $A = 36$  cells) investigated, clustering is expected to be mild, as equation (6) predicts 1 or 2 particles on average at each node. Figure 4(b) ( $N = 16 N_0$ ) indeed shows that clustering is much reduced compared with Fig. 3(b) ( $N = N_0$ ).

Clustering is most easily described in a quantitative manner by the dimensionless particle nearest-neighbor distance  $z$  calculated for each particle, from which an average value  $z_{av}$  (Fig. 5) and a distribution (Fig. 6) can be plotted as a function of time. For the standard conditions, the initial distribution, corresponding to the random location of particles before

any grain nucleates, is positively skewed and has an average value  $z_{av} = 3.5$  (Fig. 6). This value can be compared with the upper bound  $z_{av,max}$  corresponding to particles arranged on a regular lattice:

$$z_{av,max} = (c \cdot f)^{-1/2}, \quad (7)$$

where  $c$  is a geometric constant ( $c = 1$  for a square lattice,  $c = \sqrt{3}/2$  for a triangular lattice). For the standard parameters and these two geometric constants, equation (7) predicts  $z_{av,max} = 4$  and  $z_{av,max} = 4.3$ , respectively, which are, as expected, higher than the initial value  $z_{av} = 3.5$  resulting from a random distribution. The decrease of  $z_{av}$  plotted in Fig. 5 as a function of time is due to the clustering of the particles pushed by the grains as crystallization proceeds. The initial  $z$  distribution becomes broader when only a fraction of the particles have been pushed ( $t = 11$ , Fig. 6) and then narrows near the average value  $z_{av} = 1.25$  at the end of crystallization ( $t = 22$ , Fig. 6). We note that the trough in the distribution between  $z = 1.5$  and  $z = 2$  in Fig. 6 is an artifact resulting from the cellular nature of the grid: with the definition:

$$z = (a^2 + b^2)^{1/2}, \quad (8)$$

where  $a$  and  $b$  are the projected distances between the two particles on the two orthogonal axis, no value of  $z$  exists in the interval  $]\sqrt{2}; 2[$  if  $a$  and  $b$  are integers.

**4.2.2. Effect of particle mobility.** As settling occurs, particles accumulate preferentially on those grain borders which are perpendicular to, and move in the direction opposite to, the settling direction. Particle accumulation at grain borders (which is more pronounced, the larger the gap between grains [Fig. 8(a)]) inhibits the motion of grain borders as they become covered with particles. The final microstructure thus exhibits pronounced accumulation of particles at some grain triple points and near-complete depletion of particles from most grain boundaries and from those triple points resulting from particle-free borders [Fig. 8(b)]. During the course of crystallization, the average particle nearest neighbor distance  $z_{av}$  decreases more rapidly than for the case where no settling takes place, as shown in Fig. 9. In this figure, the time dependence of  $z_{av}$  is shown for increasing settling speed ( $s = 1, 3$  or  $5$  with  $N = N_0$ ) and compared with two limiting cases: (i) settling in the absence of any grain ( $s = 1, N = 0$ ) and (ii) absence of settling in the presence of grains ( $s = 0, N = N_0$ ). For short times the curves of  $z_{av}$  for  $s = 1-5$  follow that of case (i): because the grains are too small to interact significantly with the particles,  $z_{av}$  decreases as a result of random settling motion of particles. For long times the curves of  $z_{av}$  for  $s = 1-5$  tend towards that of case (ii): because settling is exhausted, the average particle nearest neighbor distance is controlled by particle pushing by borders. While the final value of  $z_{av}$  does not significantly vary with and without settling (Fig. 9), comparison of the final microstructure for  $s = 0$  (Fig. 3) and  $s = 5$

(Fig. 8) shows that clustering (when defined as the average cluster size) is much more important in the latter case.

Cluster mobility has a pronounced effect on overall particle distribution, as shown in Fig. 10 depicting the case for which clusters of at least two particles have zero mobility ( $m = 0$ ). While the average particle nearest neighbor distance is near unity (single particles are rare), the average nearest neighbor distance between clusters (most of which are particle pairs) is much larger. The majority of the pair clusters are found within grains, since these clusters are engulfed as soon as they are formed. At steady state, the number of particle pair clusters is expected to be half that of single particles and the average nearest neighbor distance between clusters is thus higher by a factor  $\sqrt{2}$  than the initial particle nearest neighbor distance. However, the region near the nucleus of each grain is depleted (because clusters start to form only after some particle pushing has taken place), while the grain boundaries are enriched both with clusters (formed when particles pushed by the two borders met) and with single particles (trapped before they formed a cluster). As expected from the lack of mobility of clusters, no particle accumulation at triple point occurs.

#### 4.3. Saturated nucleation at borders

Unlike the equiaxed grain structure resulting from isotropic continuous nucleation (Fig. 3), grains formed under saturated nucleation conditions at the edge of the field are columnar (Fig. 11), as a result of growth and impingement with neighbors. As grains growing in different directions contact along the diagonals of the field, they impinge and the number of grains decreases with time. As illustrated in Fig. 11(a), particles are pushed by the four fronts and become trapped at these grain boundary diagonals. The particles pushed by each front far from the diagonals accumulate at grain boundaries perpendicular to the front, where the clusters are still mobile [Fig. 11(b)]. The clusters, however, partially prevent the motion of the grains which can be overtaken by larger neighboring grains: this results in columnar grains ending before they reach the diagonals [Fig. 11(b)]. The final microstructure exhibits a majority of the particles trapped at grain boundary diagonals and at grain boundaries near the center, in good qualitative agreement with experimental observations during solidification of melts containing solid particles [65]. The structure is markedly different from that produced under continuous nucleation conditions [Fig. 3(b)]; fewer, larger, more elongated grains exist, with grain boundaries either completely covered with particles or completely devoid of them.

Settling further exacerbates the inhomogenous distribution of particles (Fig. 12). The front growing in the same direction as settling (but slower than the particles since  $s = 3$ ) is flat and devoid of particles [Figs 12(a, b)]. The two fronts growing in a direction

perpendicular to the settling direction push the particles and engulf only a few of them. Particles thus accumulate on the front moving in the direction opposite to the settling direction, disrupting its planarity and forming very large clusters at grain boundaries. The particles impinge more on the smaller grains, with the result that larger neighbors can overtake both the smaller grains and their associated particles. In Fig. 12(b), the number of grains growing on the particle-covered front is about half of that on fronts without particles. The final microstructure [Fig. 12(c)] exhibits a few very large particle clusters located near the "bottom" of the field and is much more inhomogeneous than for the case of continuous grain nucleation [Fig. 8(b)].

### 5. CONCLUSIONS

A two-dimensional cellular automaton model developed by Pezzee and Dunand [49, 50] for the simulation of crystallization (or alternatively recrystallization, allotropic transformation or solidification) of a matrix containing inert, immobile particles is extended to the case of mobile particles.

Particle pushing by growing matrix grains under continuous nucleation conditions is studied for different values of the following parameters: grain nucleation rate  $N$ , particle area fraction  $f$ , particle settling ratio  $s$  and particle mobility  $m$ . The crystallization kinetics and the size and shape of grains are unaffected by these parameters, with the exception of the expected decrease of grain area with increasing  $N$ . However, particle spatial distribution and particle nearest neighbor distance during and after crystallization vary widely as these parameters are changed. Particle enrichment at grain boundaries and grain triple points, which results from the trapping of particles pushed by growing grains, is reduced by increasing the grain nucleation rate and by decreasing the particle area fraction, settling ratio or mobility.

With site-saturated nucleation conditions at the boundaries of the simulation field, columnar growth of grains results, simulating e.g. solidification from container walls or recrystallization from sample edges. Strong clustering of particles takes place at grain boundaries and is further accentuated by particle settling.

*Acknowledgements*—R.K.S. and D.C.D. acknowledge the support of MIT (in the form of an Undergraduate Research Opportunity Program fellowship) and of AMAX (in the form of an endowed chair), respectively. The authors also gratefully acknowledge the financial support of NSF (grant DMR-9417636) as well as helpful discussions with Professor H. J. Frost from Dartmouth College.

### REFERENCES

1. W. A. Johnson and R. F. Mehl, *Trans. AIME* **135**, 416 (1939).
2. M. Avrami, *J. chem. Phys.* **7**, 1103 (1939).
3. M. Avrami, *J. chem. Phys.* **8**, 212 (1940).
4. A. E. Kolmogorov, *Akad. Nauk SSSR, Izv. Ser. Mat.* **1**, 355 (1937).
5. K. Marthinsen, T. Furu, E. Nes and N. Ryum, *Simulation and Theory of Evolving Microstructures* (edited by M. P. Anderson and A. D. Rollett), p. 87. TMS, Warrendale, Pennsylvania (1990).
6. V. Y. Gertsman and K. Tangri, *Acta metall. mater.* **43**, 2317 (1995).
7. T. Matsumiya, A. Nogami and H. Sawada, *Adv. Mater. Proc.* **147**, 51 (1995).
8. K. W. Mahin, K. Hanson and J. W. Morris, *Acta metall.* **28**, 443 (1980).
9. T. O. Saetre, O. Hunderi and E. Nes, *Acta metall.* **34**, 981 (1986).
10. H. J. Frost and C. V. Thompson, *Acta metall.* **35**, 529 (1987).
11. D. J. Srolovitz, G. S. Grest and M. P. Anderson, *Acta metall.* **34**, 1833 (1986).
12. A. D. Rollett, D. J. Srolovitz, R. D. Doherty and M. P. Anderson, *Acta metall. mater.* **37**, 627 (1989).
13. K. Marthinsen, O. Lohne and E. Nes, *Acta metall.* **37**, 135 (1989).
14. D. Juul-Jensen, *Scripta metall. mater.* **27**, 1551 (1992).
15. H. W. Hesselbarth and I. R. Göbel, *Acta metall. mater.* **39**, 2135 (1991).
16. P. Peczek and M. J. Luton, *Acta metall. mater.* **41**, 59 (1993).
17. V. Y. Novikov and I. S. Gavrikov, *Acta metall. mater.* **43**, 973 (1995).
18. F. J. Humphreys and M. Hatherly, *Recrystallization and Related Annealing Phenomena*, pp. 417–431. Pergamon Press, New York (1995).
19. O. Ito and E. R. Fuller, *Acta metall. mater.* **41**, 191 (1993).
20. D. J. Srolovitz, G. S. Grest, M. P. Anderson and A. D. Rollett, *Acta metall. mater.* **36**, 2115 (1988).
21. H. J. Frost, *Mater. Charact.* **32**, 257 (1994).
22. J. A. Spittle and S. G. R. Brown, *Acta metall.* **37**, 1803 (1989).
23. J. A. Spittle and S. G. R. Brown, *J. mater. Sci.* **23**, 1777 (1989).
24. Y. S. Yang, N. Blake, T. B. Abbott and J. F. McCarthy, *Scripta metall. mater.* **29**, 1285 (1993).
25. S. G. R. Brown and J. A. Spittle, *Scripta metall. mater.* **27**, 1599 (1992).
26. S. G. R. Brown, T. Williams and J. A. Spittle, *Acta metall. mater.* **42**, 2893 (1994).
27. S. G. R. Brown and N. B. Bruce, *Scripta metall. mater.* **32**, 241 (1995).
28. P. Zhu and R. W. Smith, *Acta metall. mater.* **40**, 683 (1992).
29. P. Zhu and R. W. Smith, *Acta metall. mater.* **40**, 3369 (1992).
30. M. Rappaz and C. A. Gandin, *Acta metall. mater.* **41**, 345 (1993).
31. M. Rappaz and C. A. Gandin, *MRS Bull.* **19**, 20 (1994).
32. C. Charbon, A. Jacot and M. Rappaz, *Acta metall. mater.* **42**, 3953 (1994).
33. C. A. Gandin and M. Rappaz, *Acta metall. mater.* **42**, 2233 (1994).
34. C. A. Gandin, M. Rappaz and R. Tintillier, *Metall. mater. trans.* **25A**, 629 (1994).
35. C. A. Gandin, M. Rappaz, D. West and B. L. Adams, *Metall. mater. trans.* **26**, 1543 (1995).
36. F. J. Humphreys, *Mater. Sci. Technol.* **8**, 135 (1992).
37. F. J. Humphreys, *Scripta metall. mater.* **27**, 1557 (1992).
38. F. J. Humphreys, *Mat. Sci. Forum* **113–115**, 329 (1993).
39. D. J. Jensen, *Mat. Sci. Forum* **113–115**, 335 (1993).
40. A. D. Rollett, D. J. Srolovitz, M. P. Anderson and R. D. Doherty, *Acta metall. mater.* **40**, 3475 (1992).

41. A. D. Rollett, D. J. Srolovitz, R. D. Doherty, M. P. Anderson and G. S. Grest, *Simulation and Theory of Evolving Microstructures* (edited by M. P. Anderson and A. D. Rollett), p. 103. TMS, Warrendale, Pennsylvania (1990).
42. T. Furu, K. Marthinsen, U. Tundal, N. Ryum and E. Nes, *Materials Architecture* (edited by J. B. Bilde-Sorensen, N. Hansen, D. Juul Jensen, T. Leffers, H. Lilholt and O. B. Pederson), p. 343. Risø, Roskilde, Denmark (1989).
43. T. Furu, K. Marthinsen and E. Nes, *Mat. Sci. Technol.* **6**, 1093 (1990).
44. T. O. Saetre, O. Hunderi, E. Nes and N. Ryum, *Aluminum Alloys, their Physical and Mechanical Properties* (edited by E. A. Starke and T. H. Sanders), p. 1757. EMAS, West Midlands (1986).
45. E. Nes, N. Ryum and O. Hunderi, *Acta metall.* **33**, 11 (1985).
46. N. A. Mehl and L. Rebenfeld, *J. Polym. Sci. Polym. Phys. Ed.* **31**, 1677 (1993).
47. N. A. Mehl and L. Rebenfeld, *J. Polym. Sci. Polym. Phys. Ed.* **31**, 1687 (1993).
48. N. A. Mehl and L. Rebenfeld, *J. Polym. Sci. Polym. Phys. Ed.* **33**, 1249 (1995).
49. C. F. Pezzee and D. C. Dunand, *Acta metall. mater.* **42**, 1509 (1994).
50. C. F. Pezzee and D. C. Dunand, *Crystallization and Related Phenomena in Amorphous Materials* (edited by M. Libera, T. E. Haynes, P. Cebe and J. E. Dickinson), p. 295. MRS, Pittsburgh, Pennsylvania (1994).
51. N. Vandewalle, R. Cloots and M. Ausloos, *J. mater. Res.* **10**, 268 (1995).
52. M. F. Ashby and I. G. Palmer, *Acta metall.* **15**, 420 (1967).
53. M. F. Ashby and R. M. A. Centamore, *Acta metall.* **16**, 1081 (1968).
54. E. F. Koch and K. T. Aust, *Acta metall.* **15**, 405 (1967).
55. G. Gottstein and L. S. Shvindlerman, *Acta metall. mater.* **41**, 3267 (1993).
56. M. V. Speight and G. W. Greenwood, *Phil. Mag.* **9**, 683 (1964).
57. R. L. Squires, R. T. Weiner and M. Phillips, *J. nucl. Mater.* **8**, 77 (1963).
58. J. D. Whittenberger, *Metall. Trans.* **4**, 1475 (1973).
59. A. Mortensen and I. Jin, *Int. mater. Rev.* **37**, 101 (1992).
60. P. K. Rohatgi, R. Asthana, and S. Das, *Int. metals Rev.* **31**, 115 (1986).
61. P. K. Rohatgi, R. Asthana, S. N. Tewari and C. S. Narendranath, *High Performance Composites: Commonality of Phenomena* (edited by K. K. Chawla, P. K. Liaw and S. G. Fishman), p. 93. TMS, Warrendale, Pennsylvania (1994).
62. M. C. Flemings, *Solidification Processing*, pp. 208–210. McGraw-Hill, New York (1974).
63. L. Lajoie and M. Suéry, *Cast Reinforced Metal Composites* (edited by S. G. Fishman and A. K. Dhingra), p. 15. ASM International, Metals Park, Ohio (1988).
64. E. N. Gilbert, *Ann. Math. Statist.* **33**, 958 (1962).
65. C. J. Kim, S. H. Lai and P. J. McGinn, *Mater. Lett.* **19**, 185 (1994).
66. P. K. Rohatgi, F. M. Yarandi and Y. Liu, *Cast Reinforced Metal Composites* (edited by S. G. Fishman and A. K. Dhingra), p. 249. ASM International, Metals Park, Ohio (1988).
67. D. J. Lloyd and B. Chamberlain, *Cast Reinforced Metal Composites* (edited by S. G. Fishman and A. K. Dhingra), p. 263. ASM International, Metals Park, Ohio (1988).
68. D. A. Smith, P. V. Evans and S. R. Koppikar, *Crystallization and Related Phenomena in Amorphous Materials* (edited by M. Libera, T. E. Haynes, P. Cebe and J. E. Dickinson), p. 271. MRS, Pittsburgh, Pennsylvania (1994).